Proceedings of the 7th International Symposium on Cavitation
CAV2009 – Paper No. 94
August 17-22, 2009, Ann Arbor, Michigan, USA

Prediction of cavitating flow around 3-D straight/swept hydrofoils

Sowmitra Singh
Ocean Engineering Group, The University of Texas at Austin
Austin, Texas, USA

Spyros A. Kinnas
Ocean Engineering Group, The University of Texas at Austin
Austin, Texas, USA

ABSTRACT

A boundary element method (BEM) model is applied for the prediction of cavitating flow around 3-D straight/swept hydrofoils between slip (zero shear) walls. The governing equation and boundary conditions are formulated and solved by assuming piecewise constant distribution of sources and dipoles on the hydrofoil and cavity surfaces, and piecewise constant distribution of dipoles on the trailing wake sheet. Cavity shape determination is initiated with a guessed cavity planform, and the cavity extent and thickness are determined iteratively until the dynamic and kinematic boundary conditions are satisfied on the cavity surface. To account for no-normal flow through the side walls, the method of images is used.

For the fully-wetted case, the attached flow results obtained are compared with results from a full-fledged Reynolds-Averaged Navier-Stokes (RANS) solver. The cavitating results for a straight wing between slip walls are compared with results from an existing 2-D BEM solver for cavitating flow around hydrofoils. The RANS solver is also used to study separated flow characteristics around 2-D/3-D hydrofoils at high loading.

NOMENCLATURE

C: Chord length of the 2-D hydrofoil section
C_p: Pressure coefficient, $C_p = (P - P_\infty)/(\frac{1}{2}\rho|\overrightarrow{V_{in}}|^2)$
P_v: Vapor pressure
P_∞: Far-field pressure
Re: Reynolds Number
U_i: Mean flow velocity in the i^{th} co-ordinate direction
u_i': Fluctuating flow velocity in the i^{th} co-ordinate direction
u_τ: Friction velocity, $u_\tau = \sqrt{\tau_{wall}/\rho}$
y^+: Non-dimensional wall normal co-ordinate, $y^+ = (u_\tau y)/\nu$
α: Inflow angle of attack
λ: Sweep angle of the 3-D wing/hydrofoil
ν: Kinematic viscosity of the fluid
ρ: Density of the fluid
σ: Cavitation number, $\sigma = (P - P_v)/(\frac{1}{2}\rho|\overrightarrow{V_{in}}|^2)$
τ_{wall}: Wall shear stress
ϕ: Perturbation potential

INTRODUCTION

A number of techniques have been developed in recent years to treat wetted and cavitating flow around 2-D/3-D hydrofoils. Boundary Element Method (BEM) has been found to be a computationally efficient, robust and versatile tool for analysis of such flows.

Kinnas and Fine (1991, 1993b); Fine and Kinnas (1993) have developed non-linear potential based boundary-element method for analysis of partially or super-cavitating flows around 2-D/3-D hydrofoils. Their method was extended to predict face cavitation and search for cavity detachment on three-dimensional hydrofoils and propellers by Kinnas (1998).

In the present work, a BEM model has been developed to study wetted/cavitating flow around 3-D straight/swept hydrofoils between slip walls. The BEM model is built over an existing robust numerical tool PROPCAV [PROPeller CAVitation, Kinnas and Fine (1992)]. PROPCAV is capable of analyzing 3-D unsteady flow around cavitating propellers and is based on a low-order (piece-wise constant dipole and source distribution) potential boundary element method. In the current work, to account for no-normal flow through side walls, an image model has been incorporated into PROPCAV.

Figure 1 shows the top view of a swept hydrofoil spanning between walls that are parallel to the *x-y* plane. For a straight wing between parallel walls, the sweep angle $\lambda = 0^o$ (refer Fig. 3). The two side walls are treated as no-shear or slip walls. Since the main emphasis is on predicting the influence of sweep on the hydrofoil pressure distribution, by treating the side walls as slip walls, comparisons between the inviscid 3-D BEM model and a RANS solver (Fluent[1]) are made in the absence of any tip effects that might have otherwise arisen. Furthermore, by choosing this simplistic, controlled environment, RANS calculations can be performed with a relatively lesser number of cells/elements.

[1]Version 6.3.26, Website – http://www.fluent.com/

Flow visualization experiments on wings and propeller blades at high loading show that a vortex sheet separates from the leading edge. This vortex sheet then passes over the wing or propeller blade and drastically changes the load distribution and sheet cavitation characteristics in the leading edge region of the lifting surface [Greeley (1982)]. Since future work is targeted at predicting the wetted/cavitating leading edge flow characteristics of lifting surfaces using BEM, it is very essential to obtain modeling insights by looking at leading edge viscous flow details. Choosing a controlled environment (swept wing between slip walls) is an advantage since RANS simulations can be performed with relative ease.

In this paper, the fully-wetted, attached flow results obtained from the 3-D BEM image model (PROPCAV) are compared with results from Fluent. A 2-D BEM solver for cavitating flow around hydrofoils is used to validate PROPCAV results for cavitating flow over a straight wing between slip walls. PROPCAV is also used to investigate the effect of sweep on sheet cavitation characteristics of a wing between slip walls. The RANS solver is used to study viscous separated flow characteristics of 2-D/3-D hydrofoils at high loading.

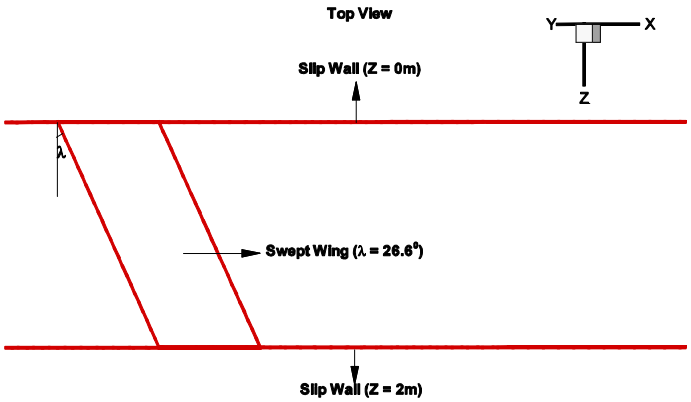

Figure 1: Top view of a 3-D swept hydrofoil spanning between two slip walls that are parallel to the x-y plane.

FORMULATION

BEM Analysis

Figure 2 shows the paneled hydrofoil geometry (without side walls) that is used for BEM analysis. Figure 3 gives the top view (*x*-*z* plane) of this geometry.

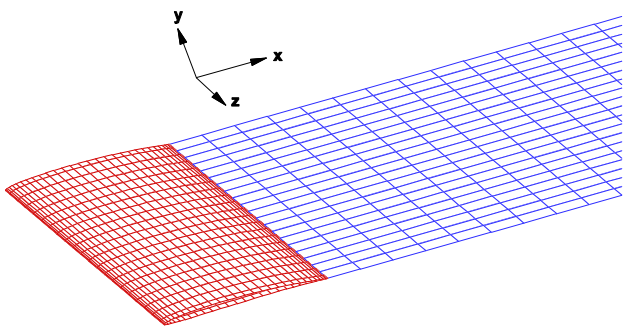

Figure 2: Paneled 3-D hydrofoil and wake geometries.

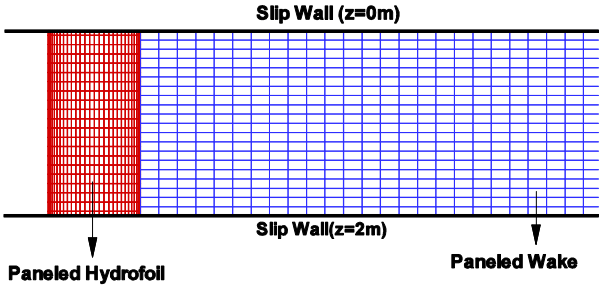

Figure 3: Top view of a paneled 3-D straight hydrofoil spanning between slip walls.

With the assumption that the fluid is inviscid and the flow is incompressible and irrotational, the total velocity, $\vec{q}(x,y,z,t)$, can be expressed in terms of the perturbation potential, $\phi(x,y,z,t)$, as follows:

$$\vec{q}(x,y,z,t) = \overrightarrow{V_{in}}(x,y,z,t) + \nabla\phi(x,y,z,t) \qquad (1)$$

$\overrightarrow{V_{in}}(x,y,z,t)$ in the above equation is the inflow velocity. The perturbation potential, $\phi(x,y,z,t)$, at any point $p(x,y,z)$ located either on the wetted blade/hydrofoil surface, $S_B(t)$, or on the cavitating surface, $S_C(t)$, has to satisfy Green's third identity.

$$2\pi\phi_p(\vec{x},t) = \int_{S_B(t)+S_C(t)} [\phi_q(\vec{x},t)\frac{\partial G(p;q)}{\partial n_q(t)} - G(p;q)\frac{\partial \phi_q(\vec{x},t)}{\partial n_q(t)}]ds + \int_{S_W(t)} \Delta\phi_w(\vec{x},t)\frac{\partial G(p;q)}{\partial n_q(t)}ds \qquad (2)$$

The subscripts, q and p, correspond to the variable and the field point, respectively. The field point is also referred to as the control point. $G(p;q) = 1/R(p;q)$ is the Green's function, where $R(p;q)$ is the distance between the field point p and the variable point q. $\overrightarrow{n_q}(t)$ is the unit vector pointing into the flow field. $\Delta\phi_w$ is the potential jump across the hydrofoil trailing wake sheet ($S_W(t)$).

With the above integral equation (Eqn. 2), the perturbation potential on the blade and cavity surfaces are determined using linear superposition of the induced potentials by the piece-wise continuous dipole and source distributions on $S_B(t) + S_C(t)$, and the potentials induced by the piece-wise continuous dipole distributions on $S_W(t)$. To account for no-normal flow through the side walls, the method of images is used. The paneled hydrofoil, cavity and wake geometries (distribution of piecewise constant sources and dipoles) are mirrored about the side walls (Fig. 4). Theoretically, to handle a geometry between two parallel walls, infinite sets of images are required. Convergence studies, however, can be carried out to determine the number of image-sets required for a fairly accurate numerical result. The source/dipole influence coefficient of a

particular panel at a control point is evaluated and the influence coefficients due to all images of this panel are added to it. The influence coefficients are normalized quantities that account for the potential induced at a field point by the source/dipole distribution at a panel. A useful detail that simplifies calculations is the fact that the source or dipole influence coefficient due to the image of a panel at a particular control point is same as the source/dipole influence coefficient due to the panel at the image of the control point in consideration (Fig. 5).

The exact solution of Eqn. 2 can be uniquely determined by applying the boundary conditions on the exact flow boundary. Since the cavity surface is unknown and to be determined as part of the solution, the boundary conditions may not be directly applied on the exact flow boundary. As mentioned in Fine (1992), the kinematic and dynamic boundary conditions for the cavity surface are applied on the approximate flow boundary, which coincides with the blade/hydrofoil surface beneath the cavity.

The boundary conditions applied to the hydrofoil, side walls, cavity and the trailing wake surfaces are as follows:

- The flow on the wetted hydrofoil is tangent to the surface.

$$\frac{\partial \phi}{\partial n} = -\overrightarrow{V_{in}}(x, y, z, t).(\vec{n}) \qquad (3)$$

- There is no-normal flow through the side walls. To account for this, the method of images as discussed earlier is used.
- Kutta condition implies that the fluid velocity at the hydrofoil trailing edge is finite.

$$|\nabla \phi| < \infty \quad \text{at the hydrofoil trailing edge} \qquad (4)$$

The iterative pressure Kutta condition [Kerwin et al. (1987); Kinnas and Hsin (1992)] that is applied, ensures the pressure equality between the suction and pressure sides of the trailing edge.

- The cavity closure condition implies that the cavity has to be closed at its end. Since the cavity planform is unknown, the boundary value problem is solved at the given cavitation number by using the guessed cavity planform which may not be closed if the pressures on the cavity planform are not corresponding to the given cavitation number. In the present method, the Newton-Raphson iterative method is adopted to find the correct cavity extent which satisfies the cavity closure condition at the given cavitation number [Fine (1992); Kinnas and Fine (1993b)].
- The dynamic boundary condition on cavity surface requires that the pressure on the cavity surface is constant and equal to the cavity/vapor pressure (P_v). The Bernoulli's equation can be manipulated to get a relation between the magnitude of the cavity velocity and the cavitation number. This relation between the magnitude of cavity velocity and the cavitation number can be used to obtain the potential on the cavity surface as described in Kinnas (1998).
- Kinematic boundary condition on the cavity surface requires the substantial derivative of the cavity surface to vanish. This boundary value problem is solved to determine the position of the cavity surface and hence the cavity height normal to the blade surface [Kinnas (1998)].
- The cavity detachment location is iteratively determined to satisfy the *smooth detachment conditions,* described in Young (2002).

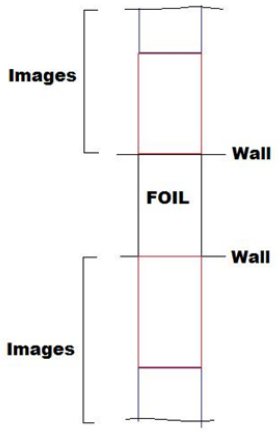

Figure 4: Top view of a 3-D straight hydrofoil mirrored about the side walls.

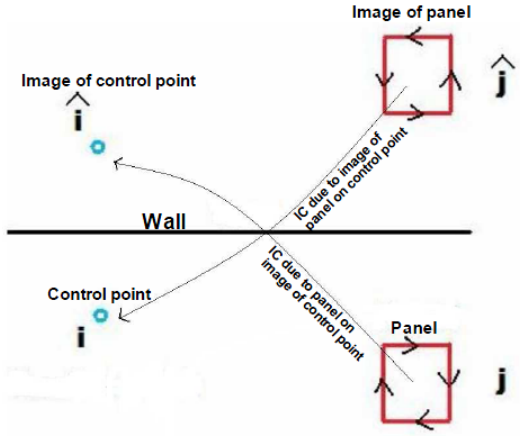

Figure 5: Influence due to the image of a panel at a control point is same as the influence due to the panel at the image of the control point.

The solution, ϕ on the wetted surface and $\frac{\partial \phi}{\partial n}$ on the cavity surface, of a boundary value problem for cavitating swept/straight hydrofoil between slip walls is determined by solving Eqn. 2 subject to boundary conditions described in the previous section.

Fluent Analysis

The domain used in Fluent to analyze flow past a swept wing is shown in Figure 6. Also shown in the figure are the relevant boundary conditions. *U* in the figure corresponds to the inflow velocity ($\overrightarrow{V_{in}}$) and α is the angle of attack. For straight wings (λ = 0^o), the domain looks similar. A 2-D mesh around the foil section in consideration is generated using 100,000 cells (Fig. 7). It is this 2-D meshed domain that is replicated along the desired direction of sweep using 25-35 stations to generate the meshed 3-D domain. The governing equations in this case are the Reynolds-Averaged Navier-Stokes (RANS) equations (Eqn. 5) along with the continuity equation (Eqn. 6).

$$\frac{\partial U_i}{\partial t} + U_j \frac{\partial U_i}{\partial x_j} = -\frac{1}{\rho}\frac{\partial P}{\partial x_i} + \frac{\partial}{\partial x_j}\left(\upsilon \frac{\partial U_i}{\partial x_j} - \left\langle u_i' u_j' \right\rangle\right) \quad (5)$$

$$\frac{\partial U_i}{\partial x_i} = 0 \quad (6)$$

Both the above equations are written using the Einstein notation. Here, $U_i$denotes the mean velocity in the i^{th} co-ordinate direction, *P* denotes the mean pressure and $\langle u_i' u_j' \rangle$ denotes the Reynolds stress terms.

The Reynolds stress model (RSM) is used for turbulence modeling in the current work. RSM closes the Reynolds-averaged Navier-Stokes equations by solving transport equations for the Reynolds stresses, together with an equation for the turbulent dissipation rate. A second-order upwind scheme is used for discretizing the equations for Momentum, Turbulent Kinetic Energy, Turbulent Dissipation Rate and the Reynolds Stresses. The pressure-velocity (momentum-continuity) coupling is done using the Semi-Implicit Method for Pressure-Linked Equations (SIMPLE). In unsteady simulations, a second order implicit scheme is used for discretization in time.

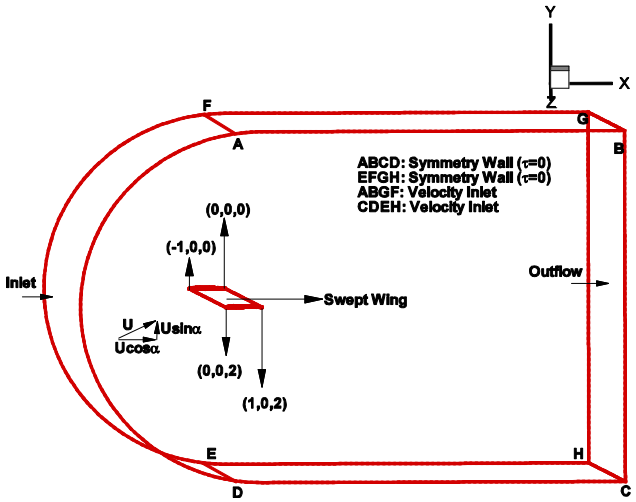

Figure 6: Domain for RANS simulation of a swept wing between slip walls.

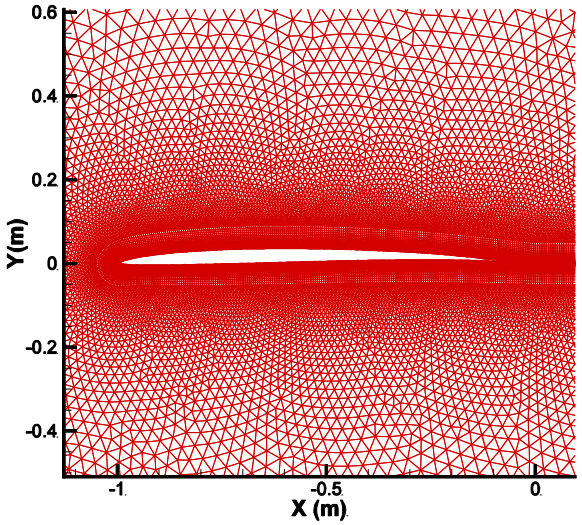

Figure 7: Mesh close to the 2-D foil section in consideration.

RESULTS AND DISCUSSION

A NACA00 (a=0.8) 2-D hydrofoil section with a chord length of 1m, maximum thickness to chord ratio (t_0/C) of 0.04 and a maximum camber to chord ratio (f_0/C) of 0.02 is used to generate the straight/swept wings that are used in the present study. All RANS calculations are performed at a Reynolds Number (*Re*) of 10^7. A turbulence length scale of 0.07C and a turbulence intensity of 0.0213 ($0.16Re^{-\frac{1}{8}}$) is used at the inlet boundary.

Fully-wetted flow

The 3-D BEM image model (PROPCAV) is used to solve for the steady fully-wetted flow past a straight wing between slip walls. The results are compared to the corresponding results from Fluent and CAV2DBL. CAV2DBL [Brewer and Kinnas (1996)] is a two dimensional BEM code capable of solving for wetted flow past a hydrofoil with/without boundary layer. The comparisons are made for an angle of attack of 5 degrees (attached flow). As expected, the result obtained from PROPCAV is completely two dimensional for this case. In other words, the flow properties remain unchanged along the *z*-direction. At this juncture, it must be mentioned that Fluent results for a 3-D straight wing between slip walls are practically identical to the Fluent results for the corresponding 2-D hydrofoil section.

Figure 8 shows a comparison of the wall pressure coefficient among Fluent (turbulent), CAV2DBL and the 3-D BEM image model (PROPCAV). Figure 9 shows a similar comparison but for a different angle of attack (α=2^0). Figure 10 gives a blow-up of Figure 9 near the leading edge of the hydrofoil. Table 1 gives C_L $[Lift/(\frac{1}{2}\rho|\overrightarrow{V_{in}}|^2 C)]$ and $C_D[Drag/(\frac{1}{2}\rho|\overrightarrow{V_{in}}|^2 C)]$ as obtained from the various methods - for α=5^0.

From Table 1, it can be seen that there is a small difference between $(C_L)_{tot}$ values of CAV2DBL (Inviscid) and PROPCAV. The small discrepancy (less than 3%) arises due to the fact that convergence of the 3-D model with the number of image sets and wake length is extremely slow. 30 image sets and a wake length of $50C$ are used for the results below. An even larger number of image sets and a longer wake are required for further reduction in error [Singh (2009)]. Because of numerical errors, values of $(C_D)_{press}/(C_D)_{tot}$ from the inviscid codes are non-zero (refer Table 1).

Figure 11 shows the wall y^+ obtained from the RANS solver. These y^+ values are within the limits prescribed in the Fluent manual[2].

	$(C_L)_{press}$	$(C_D)_{press}$	$(C_L)_{visc}$
CAV2DBL (Inviscid)	0.817754	0.000259	N/A
CAV2DBL (Viscous)	0.786553	0.001985	N/A
PROPCAV(Inviscid)	0.788377	0.000045	N/A
FLUENT (Viscous)	0.772118	0.005427	-0.000150
	$(C_D)_{visc}$	$(C_L)_{tot}$	$(C_D)_{tot}$
CAV2DBL (Inviscid)	N/A	0.817755	0.000259
CAV2DBL (Viscous)	0.005111	0.786553	0.007097
PROPCAV(Inviscid)	N/A	0.788377	0.000045
FLUENT (Viscous)	0.005528	0.771968	0.010955

Table 1: Lift and Drag coefficients (α=5^0 $-$ $steady\ run$).

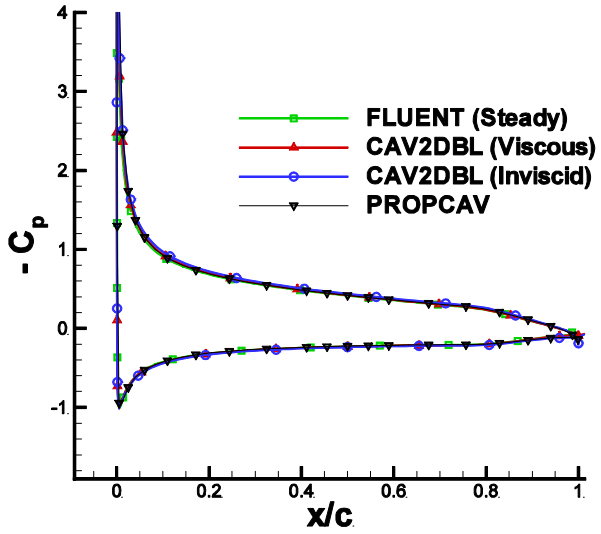

Figure 8: Comparison among Fluent (viscous), CAV2DBL and PROPCAV image model (α=5^o).

Table 2 gives the CPU time[3] for these calculations. Evidently, the BEM schemes are extremely computationally inexpensive.

Method	**CPU time**
2-D RANS simulation	6 hours with 4 processors[4]
2-D BEM (CAV2DBL)	< 1 min with 1 processor
3-D BEM Image model	< 7 min with 1 processor

Table 2: CPU time for fully-wetted calculations (straight wing).

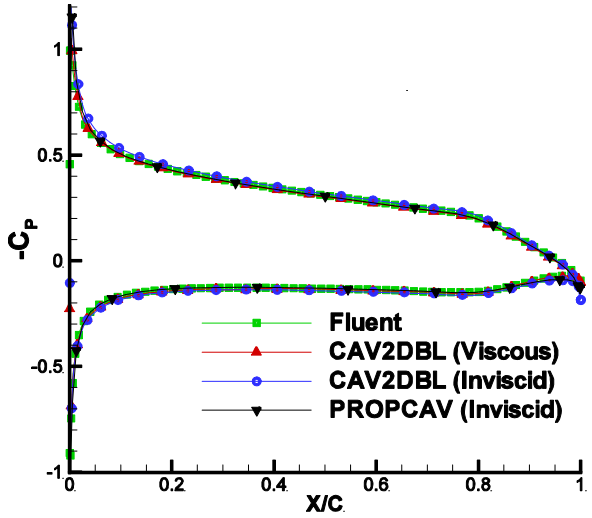

Figure 9: Comparison among Fluent (viscous), CAV2DBL and PROPCAV image model (α=2^o).

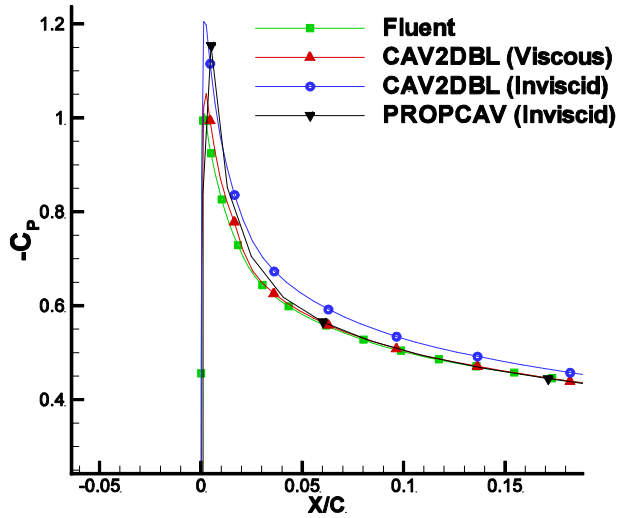

Figure 10: Comparison of pressure coefficient near the leading edge (α=2^o).

[2] Fluent 6.3 User's Guide
[3] Computer Clock time
[4] 1.6 GHz AMD Opteron, 2GB RAM

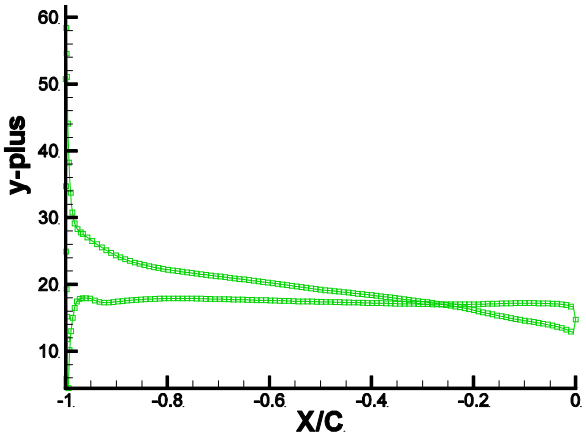

Figure 11: Wall y-plus obtained from the RANS simulation (α=5^o).

The 3-D BEM image model (PROPCAV) was further used to solve for steady fully-wetted flow past a 3-D swept wing between slip walls. The wing analyzed had a sweep of 26.6^o with respect to the z-axis (Fig. 1). The results were compared to Fluent results for this case.

Figures 12-14 present the pressure coefficient comparisons at different sections along the span of the wing. Even though Fluent is run as viscous and PROPCAV as inviscid, the pressure coefficients from the two codes compare very well. It must be noted that a viscous/inviscid interaction model [Sun (2008)] can be implemented in PROPCAV to obtain viscous flow solutions. Table 3 gives the lift coefficient (C_L) and the drag coefficient (C_D) of the swept wing as obtained from the two methods. C_L for the wing is defined as $Lift/(\frac{1}{2}\rho|\overrightarrow{V_{in}}|^2 S)$ and C_D as $Drag/(\frac{1}{2}\rho|\overrightarrow{V_{in}}|^2 S)$. Here, S denotes the planform area of the wing. Note that *Lift* and *Drag* are components of the force in the x-y plane. Comparing Fluent results from Table 3 and Table 1, it can be seen that the viscous *Drag* force does not seem to change by a great degree with sweep. This indicates that the effects of viscous *Drag* may be modeled using a constant friction coefficient.

Table 4 gives the CPU time for these calculations.

	$(C_L)_{press}$	$(C_D)_{press}$	$(C_L)_{visc}$
PROPCAV(Inviscid)	0.721468	0.000762	N/A
FLUENT (Viscous)	0.689232	0.006047	-0.000148
	$(C_D)_{visc}$	$(C_L)_{tot}$	$(C_D)_{tot}$
PROPCAV(Inviscid)	N/A	0.721468	0.000762
FLUENT (Viscous)	0.005529	0.689083	0.011576

Table 3: Lift and Drag coefficients (Swept wing, α=5^o - steady attached flow).

Method	**CPU time**
3-D RANS simulation	30 hours with 8 processors
3-D BEM Image model	< 7 min with 1 processor

Table 4: CPU time for fully-wetted calculations (swept wing).

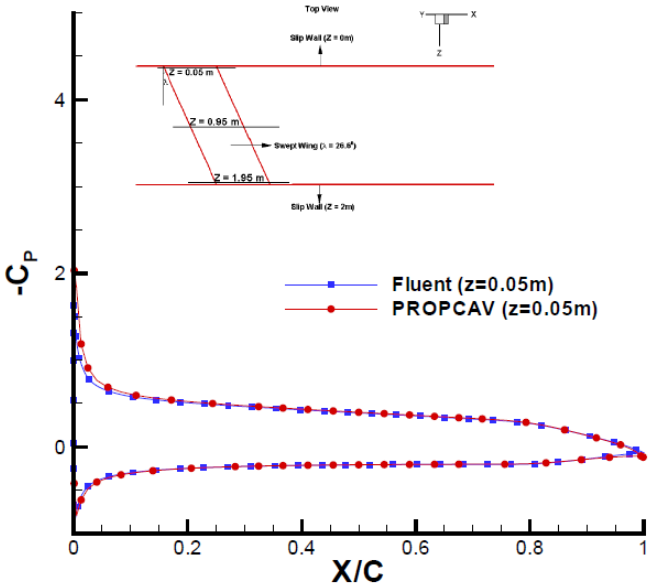

Figure 12: Comparison of pressure coefficient – PROPCAV (Image model) versus Fluent (α=5^o - steady attached flow, Z = 0.05m).

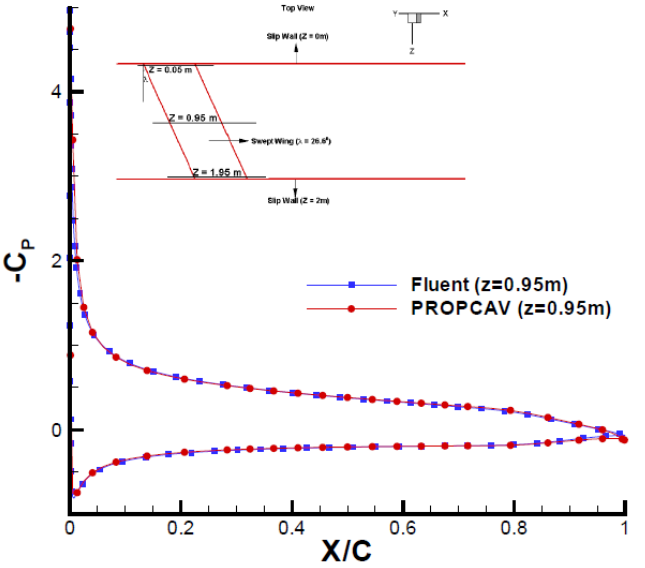

Figure 13: Comparison of pressure coefficient – PROPCAV (Image model) versus Fluent (α=5^o - steady attached flow, Z = 0.95m).

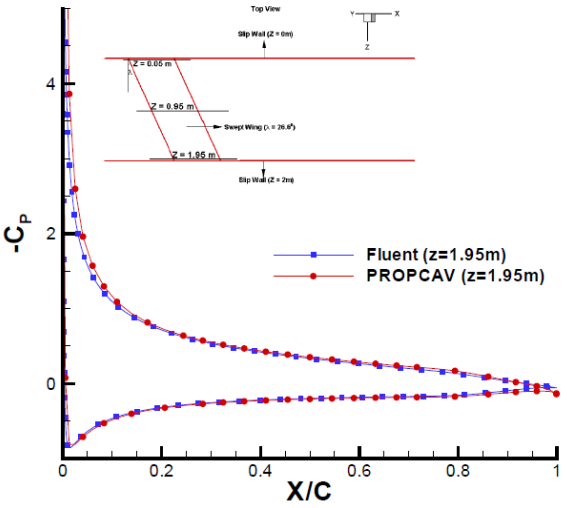

Figure 14: Comparison of pressure coefficient – PROPCAV (Image model) versus Fluent ($\alpha=5^o$ - steady attached flow, Z = 1.95m).

Cavitating flow

The cavitation model of the 3-D BEM code with images is tested by comparison with PCPAN [Kinnas and Fine (1993a)]. PCPAN in combination with CAV2DBL is used to obtain the cavitating flow solution around a 2-D hydrofoil. PROPCAV is used to solve for the flow around a straight hydrofoil between slip walls. The PROPCAV results in this case are entirely two-dimensional (no change along the *z*-direction – Fig. 21). Figure 15 shows the comparison of pressure coefficient between PROPCAV and PCPAN (σ=0.62). Figure 16 shows the 2-D cavity shapes as obtained from PROPCAV and PCPAN for this cavitation number. There is a small difference in the extents of cavities predicted by the two methods. This may be attributed to the fact that the cavity trailing edge is treated differently in the two codes. PROPCAV has a smoothing applied at the trailing edge while in PCPAN, the cavity is terminated at a panel node. Also, the number of panels that the 2-D code can afford is more.

Independent studies have been carried out by Pan (2009) to validate these 2-D BEM codes (CAV2DBL and PCPAN) by comparison with Fluent results for 2-D cavitating hydrofoils. Figures 17 and 18 [Pan (2009)] show plots of pressure coefficient obtained by 2-D BEM[5] and Fluent for two different cavitation numbers. Figures 19 and 20 [Pan (2009)] show contour plots of water vapor fraction obtained from Fluent for these cavitation numbers. Superimposed on these figures are the cavity shapes obtained from the 2-D BEM models. A mixture model for cavitation is used in Fluent for these simulations. It assumed that the cavity surface in Fluent corresponds to a contour-line on which pressure is equal to water vapor pressure. The cavity extent obtained from Fluent is taken into PCPAN as an input. In Figures 17 and 18, correction 1 is applied to the PCPAN/CAV2DBL results in order to make the pressure in the cavity region constant. Essentially, the kinematic boundary condition and the dynamic boundary condition are modified, based on the compound foil, and solved for the new cavitation number and hydrofoil potential. For the same cavity length, 2-D BEM results indicate a slightly lower cavitation number compared to Fluent results. In correction 2, the blowing source terms on the cavity surface are removed. It is observed that doing this brings the 2-D BEM results (pressure coefficient on the cavity surface) closer to the corresponding Fluent results [Pan (2009)].

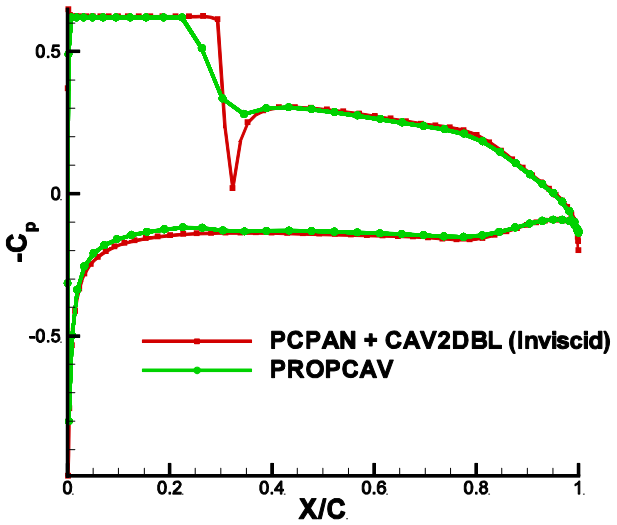

Figure 15: Comparison of pressure coefficient – PROPCAV (Image model) versus PCPAN (σ=0.62, $\alpha=2^o$- steady flow).

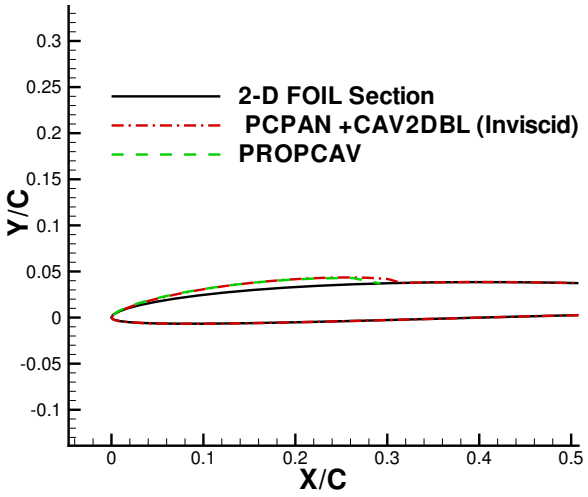

Figure 16: Comparison of cavity profiles – PROPCAV (Image model) versus PCPAN (σ=0.62, $\alpha=2^o$- steady flow).

Figure 21 gives a plot of the cavity shapes (from PROPCAV) on the straight hydrofoil along with a contour plot of the pressure coefficient (σ=0.6). It is clear from Figure 21 that the cavities are formed at locations where $-C_p$ attains a value of 0.6.

PROPCAV is also used to investigate the effect of sweep on the sheet cavity profiles of wings between slip walls. Figures 22 and 23 give the cavity profiles along with the pressure coefficient on the 3-D hydrofoil for two different

[5] PCPAN/CAV2DBL.

sweep angles (σ=0.6). Figures 24 and 25 show the pressure coefficient plots at different sections along the span of the swept hydrofoil.

From the figures, it is clear that the sheet cavities that are present on the forward region of the wing tend to shrink in size as the sweep of the wing with respect to the *z*-axis is increased. The sheet cavities on the backward swept region, on the other hand, tend to increase in extent and thickness. This is a consequence of the pressure decreasing near the wing leading edge in the backward swept region of the hydrofoil.

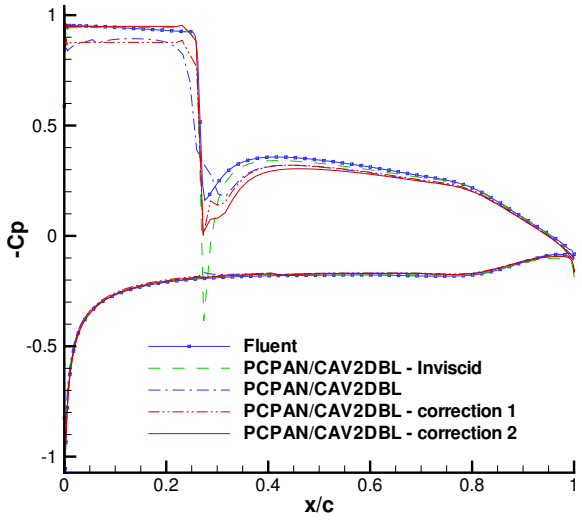

Figure 17: Comparison of pressure coefficient [Pan (2009)] – 2D BEM model versus Fluent (σ=0.955, α=3^o).

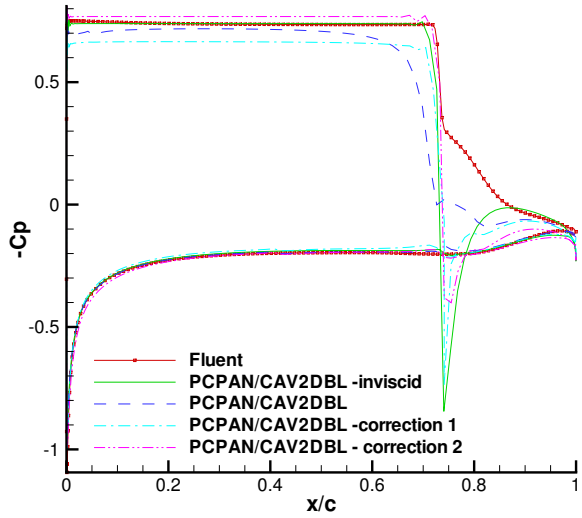

Figure 18: Comparison of pressure coefficient [Pan (2009)] – 2D BEM model versus Fluent (σ=0.754, α=3^o).

Table 5 gives the lift coefficient (C_L) and the drag coefficient (C_D) as obtained from PROPCAV for different sweep angles. C_L (wetted/cavitating) has a tendency to decrease with increasing sweep.

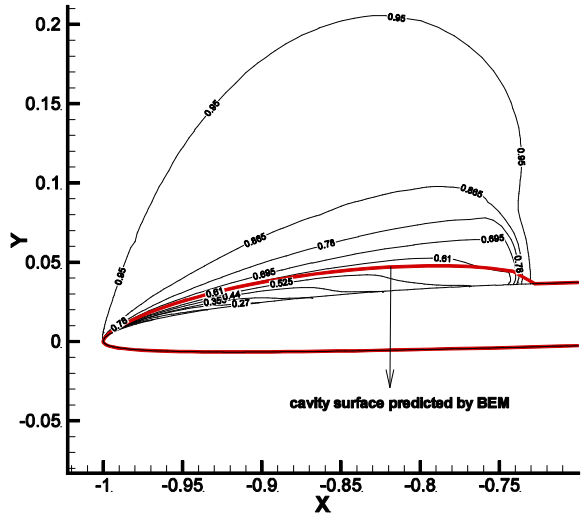

Figure 19: Water vapor fraction [Pan (2009)] - Fluent (σ=0.955, α=3^o).

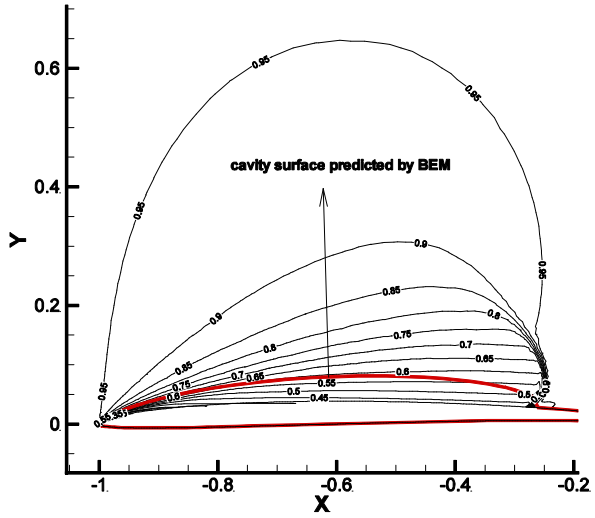

Figure 20: Water vapor fraction [Pan (2009)] - Fluent (σ=0.754, α=3^o).

λ	Wetted		Cavitating	
	(C_L)	(C_D)	(C_L)	(C_D)
0^0	0.456771	0.000311	0.473733	0.002821
15^0	0.443554	0.000447	0.462306	0.003179
26.6^0	0.414729	0.000689	0.434666	0.003489

Table 5: Lift and Drag coefficients (Swept wing, σ=0.6, α=2^o - steady flow).

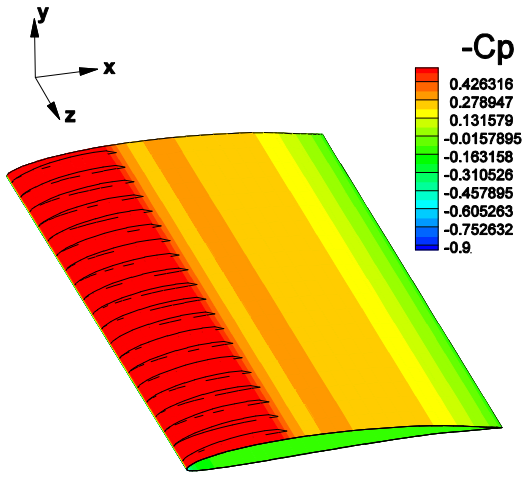

Figure 21: Cavity shapes superimposed over the contour plot of pressure coefficient on the 3-D hydrofoil (λ=0^0, σ=0.6, α=2^o- steady flow).

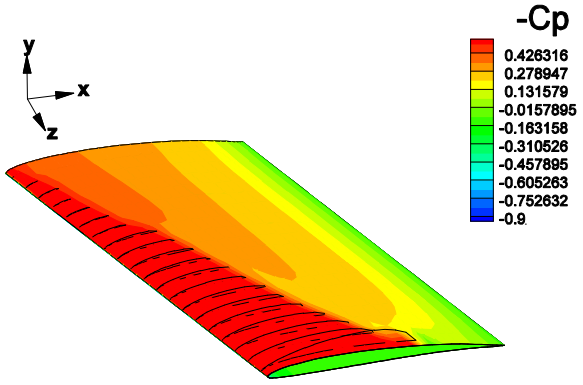

Figure 22: Cavity shapes superimposed over the contour plot of pressure coefficient on the 3-D hydrofoil (λ=15^0, σ=0.6, α=2^o- steady flow)

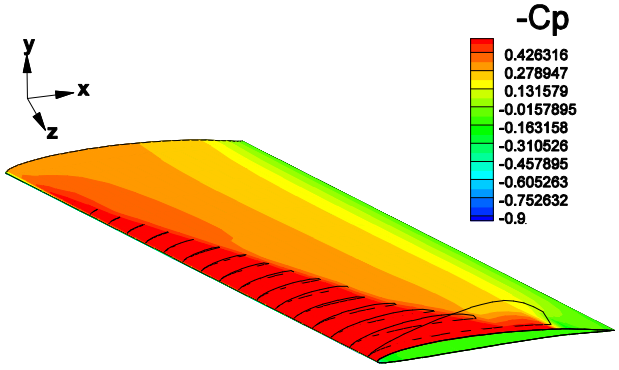

Figure 23: Cavity shapes superimposed over the contour plot of pressure coefficient on the 3-D hydrofoil (λ=26.6^0, σ=0.6, α=2^o- steady flow).

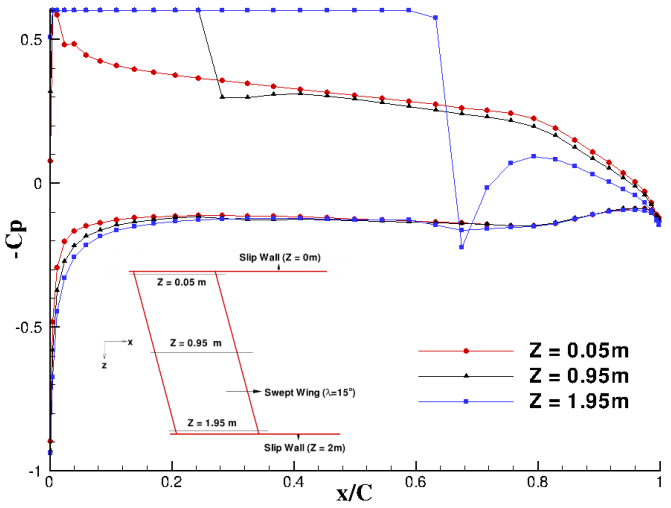

Figure 24: Pressure coefficient plots at different sections of a swept wing (λ=15^0, σ=0.6, α=2^o- steady flow).

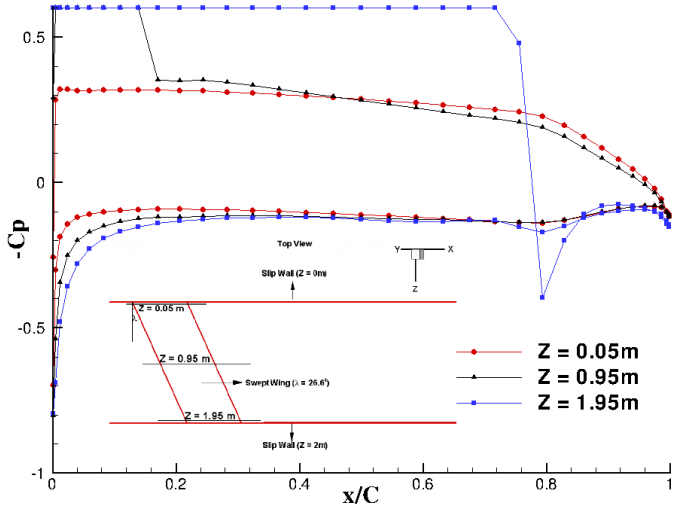

Figure 25: Pressure coefficient plots at different sections of a swept wing (λ=26.6^0, σ=0.6, α=2^o- steady flow).

Leading Edge Flow Breakdown

At high loading the fully-wetted and cavitating flow characteristics around lifting surfaces change considerably due to leading edge flow separation. The effect of this leading edge vortex can be modeled using BEM once the viscous flow details around the leading edge region are available. The shape of this shed vortex sheet can be modeled using a force free condition as described in Lee and Kinnas (2004).

Unsteady fully-wetted Fluent simulations were used to capture leading edge flow breakdown in 2-D hydrofoils and 3-D swept wings. For the 2-D foil section in consideration (NACA00), the flow breakdown first occurs at angle of attack of 8^0.

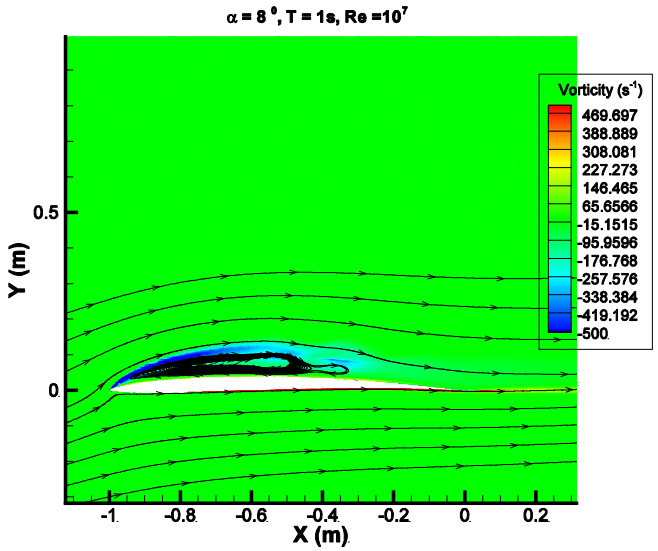

Figure 26: Flow streamlines superimposed over the vorticity contour plot for a 2-D hydrofoil (α=8^o, T =1s, Re=10^7).

Figure 26 shows the vorticity contour plot for flow around a 2-D hydrofoil (α=8^o). The plot generated after a simulation time (T) of 1s, clearly captures the leading edge recirculation zone.

Figure 27 gives the pressure coefficient at different sections of a swept wing that is subjected to a high angle of attack (α=12^o). Also plotted on this figure is the pressure coefficient obtained from the 2-D simulation for this section. The regions of constant pressure indicate recirculating flow. Figure 28 gives the contour plot of pressure coefficient on the entire swept wing. Table 6 gives the CPU time for these simulations.

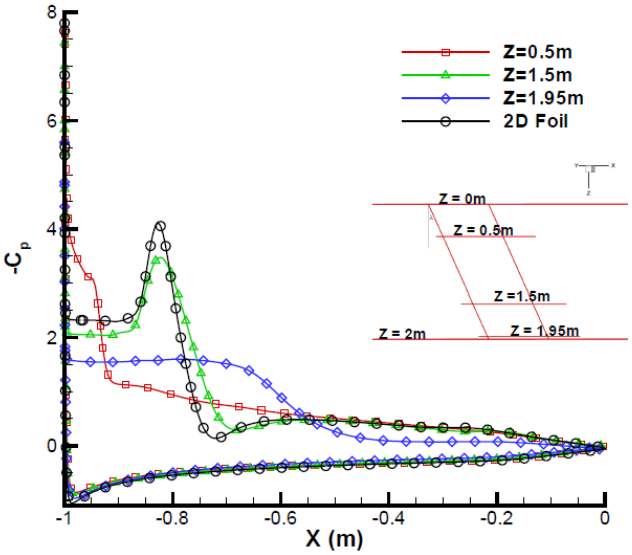

Figure 27: Pressure coefficient plots at different sections of a swept wing (λ=26.6^0, α=12^o, T=0.2s, Re =10^7).

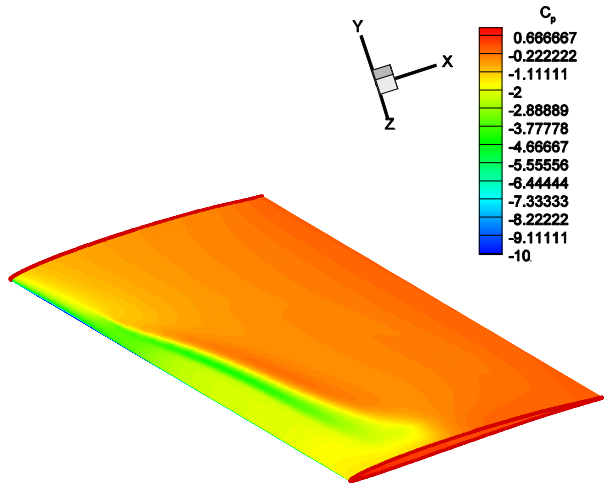

Figure 28: Pressure coefficient plot- entire wing (λ=26.6^0, α=12^o, T=0.2s, Re =10^7). Note: Presence of a leading edge vortex can be seen through its trace on the pressure distribution.

Method	CPU time
2-D unsteady (RANS)	10 hours for 100 simulation time steps with 4 processors [time step size (Δt)=0.002s]
3-D unsteady (RANS)	30 hours for 50 simulation time steps with 4 processors [time step size (Δt)=0.002s]

Table 6: CPU time for high angle of attack RANS calculations.

CONCLUSION

Attached flow results obtained from the 3-D BEM image model (PROPCAV) for straight/swept wings between slip walls compare well with the corresponding results from Fluent. The CPU-times for simulations clearly suggest that BEM calculations are extremely computationally inexpensive when compared to full-fledged RANS calculations.

Cavitating results for a straight wing between slip walls agree well with the results from PCPAN and CAV2DBL. Also, the flow properties in this case are verified to be perfectly two-dimensional.

PROPCAV is also used to investigate the effect of sweep on sheet cavitation characteristics of a wing between slip walls. The leading edge pressure is found to decrease in the backward region of the swept hydrofoil causing larger cavities. It is hard to evaluate these results as experimental results are not available.

The RANS solver (Fluent) is used to study viscous separated flow characteristics of 2-D/3-D hydrofoils at high loading. Future work is targeted at using the leading edge viscous flow details to develop a BEM model for prediction of wetted/cavitating flow around lifting surfaces at very high loading.

ACKNOWLEDGMENTS

Support for this research was provided by the U.S. Office of Naval Research (contract N00014-07-1-0616) and Phase V of the "Consortium on Cavitation Performance of High Speed Propulsors" with the following members: American Bureau of Shipping, Daewoo Shipbuilding & Marine Engineering Co. Ltd., Kawasaki Heavy Industries Ltd., Naval Surface Warfare Center Carderock Division, Rolls-Royce Marine AB, Rolls-Royce Marine AS, Samsung Heavy Industries Co. Ltd., SSPA AB, VA Tech Escher Wyss GmbH, Wärtsilä Propulsion Netherlands BV, Wärtsilä Propulsion AS, Wärtsilä CME Zhenjiang Propeller Co. Ltd. and Wärtsilä Lips Defense S.A.S.

The authors also acknowledge the efforts of Mr. Yulin Pan of the Ocean Engineering Group at UT Austin in providing 2-D correlations between CAV2DBL and Fluent for cavitating flows.

REFERENCES

[1] Brewer, W. and Kinnas, S. (1996). CAV2DBL (cavitating 2-dimensional with boundary layer) user's manual (version 1.0). Technical report, Department of Ocean Engineering, Massachusetts Institute of Technology.

[2] Fine, N. E. (October 1992). *Nonlinear Analysis of Cavitating Propellers in Nonuniform Flow.* PhD thesis, Department of Ocean Engineering, Massachusetts Institute of Technology.

[3] Fine, N. E. and Kinnas, S. (1993). A boundary element method for the analysis of the flow around 3-D cavitating hydrofoils. *Journal of Ship Research*, 37:213-224.

[4] Greeley, D. S. (1982). *Marine Propeller Blade Tip Flows.* PhD thesis, Department of Ocean Engineering, Massachusetts Institute of Technology.

[5] Kerwin, J. E., Kinnas, S. A., Lee, J. -T., and Shih, W. – Z. (1987). A surface panel method for the hydrodynamic analysis of ducted propellers. *Transactions of Society of Naval Architects &Marine Engineers,* 95.

[6] Kinnas, S. (1998).The prediction of unsteady sheet cavitation, *in,* 'Third International Symposium on Cavitation', Grenoble, France.

[7] Kinnas, S. and Fine, N. E. (1991). Non-Linear Analysis of the Flow Around Partially or Super-Cavitating Hydrofoils by a Potential Based Panel Method, *in*, 'Boundary Integral Methods-Theory and Applications, Proceedings of the IABEM-90 Symposium', Rome, Italy, October 15-19, 1990, pages 289-300, Heidelberg. Springer-Verlag.

[8] Kinnas, S. A. and Fine, N. E. (1992). A nonlinear boundary element method for the analysis of unsteady propeller sheet cavitation, *in,* 'Nineteenth Symposium on Naval Hydrodynamics', Seoul, Korea, pp. 717-737.

[9] Kinnas, S. A. and Hsin, C, -Y. (1992). A boundary element method for the analysis of the unsteady flow around extreme propeller geometries. *AIAA Journal*, 30(3):688-696.

[10] Kinnas, S. A. and Fine, N. E. (1993a). MIT-PCPAN and MIT-SCPAN User's Manual, Version 1.0 the Analysis of Partially Cavitating Hydrofoils.

[11] Kinnas, S. A. and Fine, N. E. (1993b). A numerical nonlinear analysis of the flow around two- and three-dimensional partially cavitating hydrofoils. *Journal of Fluid Mechanics*, 254:151-181.

[12] Lee, H. S. and Kinnas, S. A. (2004). Application of boundary element method in the prediction of unsteady blade sheet and developed tip vortex cavitation on propellers. *Journal of Ship Research* 48(1), 15-30.

[13] Pan, Y. (2009). *A Viscous/Inviscid interactive approach and its applications to wetted or cavitating hydrofoils and propellers with non-zero trailing edge thickness.* Master's thesis, Ocean Engineering Group, Department of Civil, Architectural and Environmental engineering, The University of Texas at Austin.

[14] Ridder, S. O. (1974). Experimental studies of the Leading Edge Suction Force, *in* 'International Council of the Aeronautical Sciences Proceedings', Haifa, Israel.

[15] Singh, S. (2009). *Viscous/Inviscid flow around 2-D and 3-D Hydrofoils with emphasis on Leading Edge Flow Separation.* Master's thesis, Ocean Engineering Group, Department of Civil, Architectural and Environmental engineering, The University of Texas at Austin.

[16] Sun, H. (2008). *Performance Prediction of Cavitating Propulsors using a Viscous/Inviscid Interaction Method (also UT-OE Report No. 08-2)*. PhD thesis, Ocean Engineering Group, Department of Civil, Architectural and Environmental engineering, The University of Texas at Austin.

[17] Young, Y. L. (2002). *Numerical Modeling of Supercavitating and Surface-Piercing Propellers (also UT-OE Report No. 02-1)*. PhD thesis, Ocean Engineering Group, Department of Civil, Architectural and Environmental engineering, The University of Texas at Austin.